

PAPER

Fast Fog Detection for De-Fogging of Road Driving Images

Kyeongmin JEONG[†], Kwangyeon CHOI[†], Donghwan KIM[†], *Nonmembers*, and Byung Cheol SONG^{†a)}, *Member*

SUMMARY Advanced driver assistance system (ADAS) can recognize traffic signals, vehicles, pedestrians, and so on all over the vehicle. However, because the ADAS is based on images taken in an outdoor environment, it is susceptible to ambient weather such as fog. So, preprocessing such as de-fog and de-hazing techniques is required to prevent degradation of object recognition performance due to decreased visibility. But, if such a fog removal technique is applied in an environment where there is little or no fog, the visual quality may be deteriorated due to excessive contrast improvement. And in foggy road environments, typical fog removal algorithms suffer from color distortion. In this paper, we propose a temporal filter-based fog detection algorithm to selectively apply de-fogging method only in the presence of fog. We also propose a method to avoid color distortion by detecting the sky region and applying different methods to the sky region and the non-sky region. Experimental results show that in the actual images, the proposed algorithm shows an average of more than 97% fog detection accuracy, and improves subjective image quality of existing de-fogging algorithms. In addition, the proposed algorithm shows very fast computation time of less than 0.1ms per frame.

key words: fog, haze, detection, road, driving, de-hazing

1. Introduction

The advanced driver assistance systems (ADAS) are needing more and more image processing and computer vision algorithms. For instance, computer vision algorithms to detect nearby vehicles, pedestrians, and signs already became an important technology for protecting the safety of the driver and the surrounding pedestrians.

On the other hand, since such a technology usually adopts images taken in outdoors such as a road driving environment, its detection performance is susceptible to the surrounding environment. In bad weather conditions such as fog, rain, and snow, the image quality is deteriorated, and the performance of conventional object recognition algorithms is normally degraded. Thus, various fog removal algorithms have been proposed to solve this problem [1]–[7].

However, if the conventional de-fogging algorithm such as [6] is applied to a foggy image obtained under a road driving environment, the contrast of the image is excessively improved and the adverse effect of darkening the image occurs as in Fig. 1. Also, we can observe color distortion in the wide sky area. If the de-fogging algorithm is applied to a fogless image, as shown in Fig. 2, the color distortion can

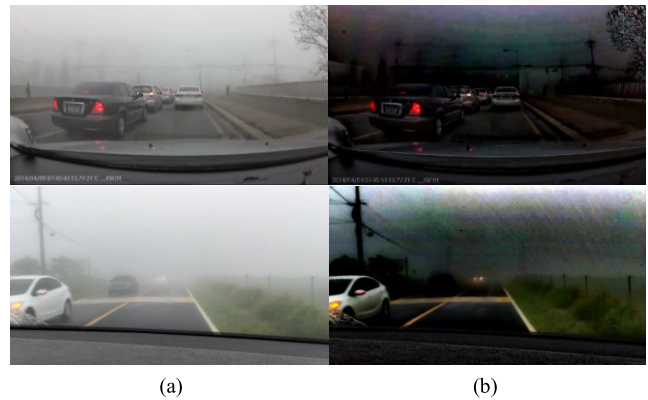


Fig. 1 Examples of excessive contrast enhancement. (a) Input fog images and (b) defogging results of (a) with Berman's method [6].



Fig. 2 Examples of color distortion. (a) Fog-free images (b) defogging results of (a).

be often observed.

In order to mitigate or solve the problems, fog detection may be considered as a pre-processing prior to fog removal step. Recently, various fog detection algorithms have been proposed [8]–[16]. Conventional fog detection algorithms require camera environment information or require prior learning. On the other hand, most existing fog detection algorithms are not suitable for real-time applications because they have considerable computation time. In addition, since those algorithms are targeting general images, their accuracy can deteriorate in the road images.

In this paper, we propose a fast and accurate single-image-based fog detection algorithm for road driving images that works without any learning process. We extract

Manuscript received July 5, 2017.

Manuscript revised September 25, 2017.

Manuscript publicized October 30, 2017.

[†]The authors are with the Department of Electronics Engineering, Inha University, Republic of Korea.

a) E-mail: bcsong@inha.ac.kr

DOI: 10.1587/transinf.2017EDP7211

features for fog detection every frame and apply a temporal filter to the extracted features to achieve fairly stable and accurate fog detection.

We also propose a metric to measure the degree of fog in order to avoid excessive contrast enhancement during fog removal. Finally, after the fog detection, the sky and non-sky regions are divided and different fog removal techniques are applied to the two regions so as to prevent the color distortion in the sky region. On the other hand, the proposed algorithm is suitable for real-time de-fogging system because it has a very small amount of computation compared to the conventional methods.

The organization of this paper is as follows: Section 2 describes conventional fog detection and fog removal algorithms. Section 3 describes the proposed fog detection algorithm in detail. Section 4 evaluates the proposed method. Section 5 concludes this paper.

2. Related Works

Conventional fog detection algorithms define fog when horizontal visibility is below a certain distance. It is called ‘visibility distance.’ Busch et al. presented a new technique to estimate the visibility distance in a foggy condition, which is based on a psychovisual model and on contrast estimation using wavelet transform [9]. Caraffa et al. [10] calculated a slightly more accurate meteorological visibility. The meteorological visibility is calculated from Eq. (1) from Duntainy attenuation law according to the International Commission on Illumination (CIE) that the contrast of the object should be higher than 5%.

$$d_{met} = \frac{-\ln(0.05)}{\beta} \quad (1)$$

where d_{met} indicates meteorological visibility.

Hautiere et al. and Mao et al. have detected fog based on the Koschmieder’s law model [11], [12]. Hautiere et al.’s method estimated the depth by modeling the environment in which the camera is installed [11]. Mao et al. estimated the fog factor and detected fog using the property that the difference between the maximum value and the minimum value of the RGB color channel is larger as the fog becomes darker [12]. Ancuti et al. proposed a semi-inverse method to detect fog-containing regions [13]. In Liu et al.’s algorithm, the histogram of each channel is analyzed in the HSV color model and determined a proper threshold value to detect the fog [14]. Bronte et al. detected fog by using a property that fog weakens the edge strength [15]. Alami et al. used the correlation between saturation and RGB color channel in the HSV color model [16]. Pavlic et al. trained features based on the power spectrum of the image through SVM [8]. The above-mentioned fog detection algorithms utilize pre-training information as well as self-information of input images, and have limitations that sometimes require specific hardware. Furthermore, as the pre-processing of the real-time fog removal system they show heavy computational time of more than several tens of ms per frame on a gen-

eral PC environment.

Usually, de-fogging procedure will be followed after fog detection. A lot of de-fogging algorithms are based on the following Koschmieder law model. On RGB color format, a foggy image can be modelled by Eq. (2).

$$I_c(\mathbf{x}) = t(\mathbf{x})J_c(\mathbf{x}) + (1 - t(\mathbf{x}))A_c, \quad c \in \{R, G, B\} \quad (2)$$

where \mathbf{x} indicates a pixel location, and A_c stands for atmospheric light value, and $t(\mathbf{x})$ means transmission value. Also, $I_c(\mathbf{x})$ and $J_c(\mathbf{x})$ indicate a foggy pixel value and its corresponding fog-free pixel value, respectively. The light scattering by the fog particles becomes stronger as the distance between them increases. So transmission values are modeled such that the weight decreases as the distance increases (see Eq. (3)).

$$t(\mathbf{x}) = e^{-\beta d(\mathbf{x})} \quad (3)$$

where β and $d(\mathbf{x})$ denote scattering coefficient and scene depth at \mathbf{x} , respectively. The latest de-fogging algorithms try to estimate the atmospheric light values and transmission values from only a single image.

He et al. proposed a simple but effective ‘dark channel prior’ to remove fog from a single input image [4]. It is based on a key observation that most local patches in outdoor fog-free images contain some pixels whose intensity is very low in at least one color channel. Using this, their method could recover high quality fog-free images. Kim et al. estimated the transmission value by defining a cost function that divides a foggy image into patches of a certain size and maximizes the contrast of each patch [5]. The atmospheric light value is obtained by dividing the image into four equal parts, finding the area with the minimum variance value, and then finding the largest RGB value in the area. Berman et al. [6] used the property that it is possible to approximate an image with RGB values with distinct color values in a fog-free image. In the foggy images, pixels with distinct color values form a so-called fog line around the atmospheric light, which is used to estimate the transmission value.

3. Proposed Algorithm

Figure 3 describes the overview of a de-fogging scheme including the proposed fog detection algorithm. The first step is to detect fog efficiently. It is necessary to examine the regions over a certain distance. In the general road driving image(s), the upper part is usually the sky area and the lower part is normally the road area. If so called ‘vanishing point’ is assumed to be known, the actual distance becomes closer the further from the vanishing point. So, in order to detect fog, we set the region of interest (ROI) over a certain distance centered on the vanishing point. In this paper, we find the driving lanes in the input image and draw their extension lines, and decide the point where the two extension lines cross as the vanishing point. That is, the vanishing point was manually determined for the ideal setting. On the other hand, the location of the vanishing point

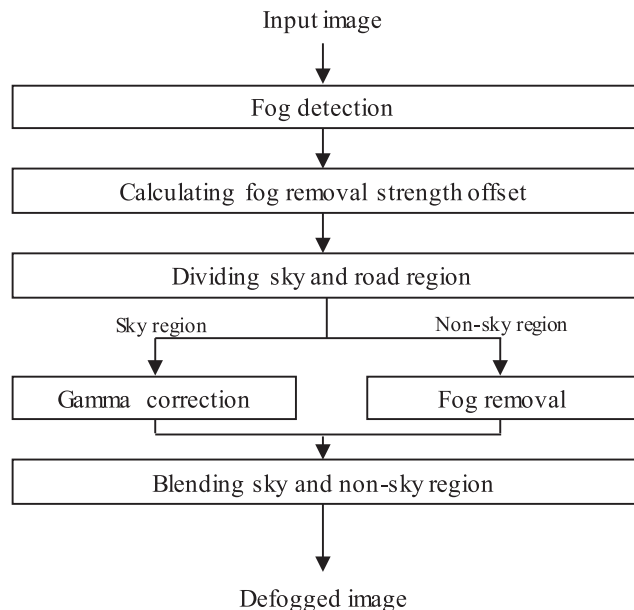


Fig. 3 The overview of a de-fogging scheme including the proposed fog detection algorithm.

in road driving images is rarely changed. Considering the above-mentioned characteristics, we did not decide vanishing point every frame and decided at 5 second interval manually. Of course, automatic detection algorithm like [17] can be adopted to detect such vanishing points. Then, the ratio of saturation (S) and value (V) in the HSV color model domain is calculated within the set ROI. This feature is mainly used for fog detection. On the other hand, sudden change of road environment may make some computed S/V ratios outliers. Using the property that fog does not disappear suddenly or does not appear, we greatly reduce outliers by applying temporal filtering to S/V ratios.

Second, the fog density is estimated using the S/V ratios. According to the estimated fog density, the strength of fog removal is adjusted to achieve effective fog removal without artifacts.

Third, since the road driving image includes a lot of sky areas, it is generally brighter than the natural image. So, when the de-fogging algorithm based on contrast enhancement is directly applied to the road driving image, the brightness of the specific area can be greatly deteriorated. Therefore, each image or frame is divided into the sky and non-sky regions, and those regions are processed independently. In case of road images, the sky is generally very bright or has blue color, so its B-channel values on the RGB space tend to be large. So we can detect the sky area by comparing the B channel values with a specific threshold.

Next, the conventional gamma correction is applied to a generally meaningless divided sky area. On the other hand, non-sky areas include roads and vehicles that are a major area of interest, so a specific fog removal algorithm is applied.

Finally, a single image is created by blending the

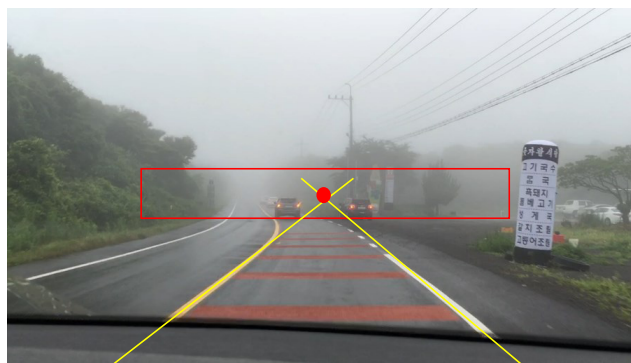


Fig. 4 Vanishing point detected manually and region of interest for fog detection.

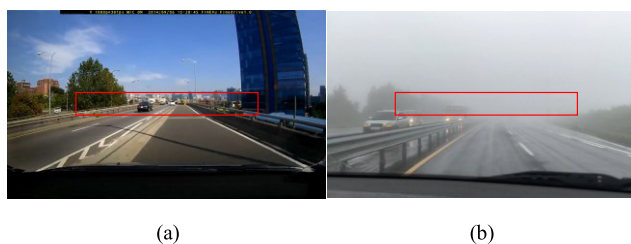


Fig. 5 Examples of V/S ratios. (a) Fog-free image $R(f_i) = 1.02$ (b) foggy image $R(f_i) = 13.32$.

gamma-corrected sky area and the fog-removed non-sky area. Here, a typical alpha blending technique is applied so that the boundary between the regions is not visible.

The following subsections describe each step in detail.

3.1 Fog Detection with Temporal Filtering

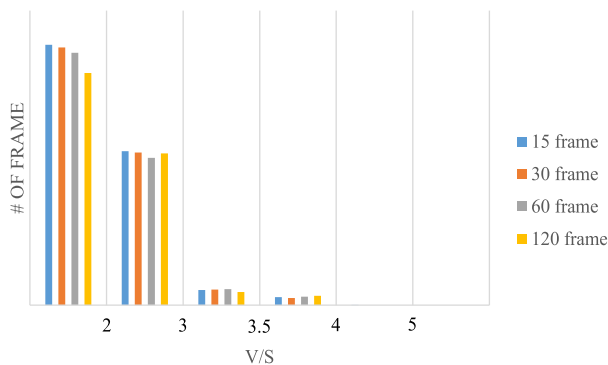
Assume that a vanishing point is already estimated by a certain method, and an ROI of a specific distance or more is pre-set. For example, for an input image with a resolution of 1280x720, the size of the ROI can be set to 720x80 around the vanishing point detected manually as shown in Fig. 4. The yellow line is the extension of the lane, the red point is the vanishing point, and the red box is the ROI.

If the color inside the ROI is not clear, S value of the HSV color model tends to be small. Also, because a foggy ROI has relatively light gray, it tends to have a large V value. For these reasons, V/S in the foggy ROI will be large. Thus, we can define the ratio of S and V as a feature to judge the presence of fog like Eq. (4).

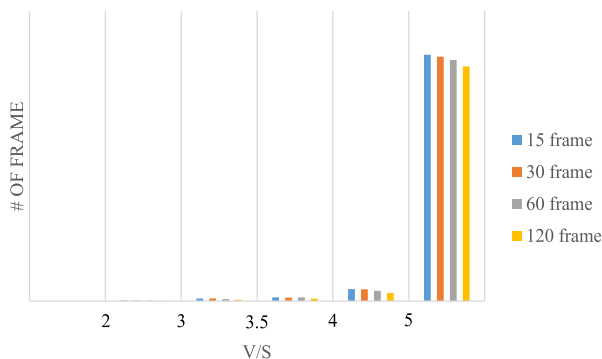
$$R(f_i) = V(f_i)/S(f_i) \tag{4}$$

where f_i indicates the ROI of the i -th frame. In Eq. (4), $V(f_i)$ and $S(f_i)$ stand for the average V and S values. Figure 5 shows an example.

However, a certain frame in a video sequence may not show the above-mentioned characteristic due to various causes. Fortunately, without loss of generality, fog does not appear or disappear suddenly. So, we adopt this property via temporal averaging as shown in Eq. (5).



(a)



(b)

Fig. 6 The histograms of V/S ratios. (a) Fog-free video (b) foggy video

$$R_j = \frac{1}{W} \sum_{i=j-W+1}^j R(f_i) \quad (5)$$

where R_j indicates the temporal averaging result for the j -th frame. W stands for the temporal window size.

Finally, R_j is compared with a threshold for fog detection. If R_j is greater than the threshold, the j -th frame is a foggy frame. Otherwise, it is a fog-free frame. In this paper, the threshold was empirically set to 3.5. The experimental proof for determining the stable threshold is given as follows:

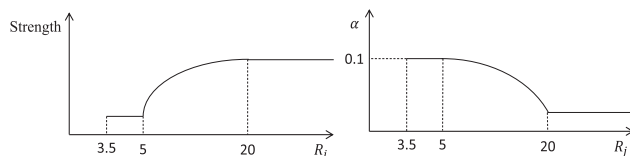
For this experiment, we acquired a total of 3,000 frames, which are different from the test frames in Sect. 4. Half of the video frames is fog-free, and the rest are foggy images. First, to investigate the effect of temporal filter window (W) on the performance, we performed the following experiment for several W values of 15 frames, 30 frames, 60 frames, and 120 frames. Figure 6 shows the histograms for the computed R_j values. The V/S ratio tends to be very small when there is no fog, and it becomes increasing for foggy images. Based on the observation in Fig. 6, we could set the threshold for fog detection to 3.5 experimentally without respect to W .

3.2 Calculation of Fog Removal Strength Offset

In general, the fog concentration or density affects the de-

Table 1 Averages of V/S

| Org | Visibility distance [m] | | | | | | |
|-----|-------------------------|------|------|------|-------|-------|--------|
| | 400 | 300 | 250 | 200 | 150 | 100 | 50 |
| 4.6 | 35.3 | 48.5 | 60.9 | 83.2 | 132.6 | 300.3 | 2467.8 |



(a)

(b)

Fig. 7 Graph of transmission offset. (a) R_j and strength (b) R_j and α .

gree of light scattering caused by fog particles. Accordingly, the V/S ratio may change depending on the fog density. To demonstrate this phenomenon experimentally, foggy images corresponding to all the fog-free images of Sect. 4 were synthesized according to visibility distance by using SiVICTM software [18], [19]. Table 1 shows the average V/S ratios for all the test images according to visibility distances. Here, ‘Org’ indicates a fog-free case. Note that the V/S ratios are very large in the synthesized foggy images. The lower the visibility distance, the higher the V/S ratio. As a result, since the fog density is proportional to the V/S ratio, it can be estimated from V/S ratio derived by Eq. (5).

On the other hand, the de-fogging strength in the following fog removal step needs to be adjusted according to the fog density. Note that conventional de-fogging algorithms work according to the transmission value, i.e., the depth information as in Eq. (1) and Eq. (2). So, by adjusting the transmission value of the ROI depending on the fog density, the fog removal strength can be further controlled. In this paper, we define the fog density-dependent offset experimentally, and apply it to the transmission value. Details of the offset determination process is as follows:

For the experiment to measure fog density according to the R_j value, ten men in their 20s were employed as the subjects. For this experiment, 3,000 test images used in the previous subsection were adopted again. For $5 \leq R_j \leq 20$, the subjects feel that the fog density which the experimenters perceive is proportional to R_j . However, when the R_j was more than 20, they thought that the fog density does not increase any more. Further, when R_j was 5 or less, it was judged that there was little fog. As a result, the fog density that a person feels according to R_j can be modeled like Fig. 7 (a).

Based on this model, transmission values can be adjusted via offsets to control the following fog removal strength as shown in Eq. (6).

$$t'(\mathbf{x}) = t(\mathbf{x}) + \alpha \quad (6)$$

Note that α can be easily modeled by reversing Fig. 7 (a) (see Fig. 7 (b)). The offset α can be defined by Eq. (7).

$$\alpha = \begin{cases} 0.1 & R_j < 5 \\ \lambda \exp(-(R_j - 5)^2 / 2\sigma_r^2) & 5 < R_j \leq 20 \\ 0.0755 & R_j > 20 \end{cases} \quad (7)$$

where λ is a constant to decide the maximum offset and σ_r indicates a variance for transmission offset control. In this paper, λ and σ_r were empirically set to 0.1 and 20, respectively. Those values were equivalently applied to all the frames.

3.3 Sky Detection and Region-Adaptive De-Fogging

Generally, the flat sky area in road images tends to be strongly contrast-enhanced because its transmission value is very small. As a result, color distortion or noise boosting often occurs in the sky region as shown in Fig. 1.

To prevent this phenomenon(s), each image is partitioned into the sky region and the non-sky region, and two different fog removal techniques are separately applied. In the day-time road images, the sky region is generally very bright or blue. Therefore, as shown in Eq. (8), the sky region is detected on a pixel basis by comparing the B channel value with a specific threshold θ_B on the RGB color space.

$$I_{SKY}(\mathbf{x}) = \begin{cases} I_c(\mathbf{x}) & , I_B(\mathbf{x}) \leq \theta_B \quad (c \in \{R, G, B\}) \\ 0 & , I_B(\mathbf{x}) > \theta_B \end{cases} \quad (8)$$

where $I_{SKY}(\mathbf{x})$, $I_c(\mathbf{x})$, and $I_B(\mathbf{x})$ indicate the sky region, the input color image, and the input B channel image, respectively. In this paper, θ_B was empirically set to 150. On the other hand, the sky region in the road images is generally located above the vanishing point. Using this characteristic together, the sky regions (white) such as Fig. 8 (b) are detected. Since the sky region has meaningless information from the perspective of the ADAS system, $J_{SKY}(\mathbf{x})$ is generated by only applying the gamma correction, which is the most basic contrast enhancement technique.

On the other hand, by applying the normal de-fogging algorithm to the non-sky region together with the offset value in Sect. 3.2, a fog removed non-sky image $J_{Non-SKY}(\mathbf{x})$ is generated like Eq. (9).



(a) (b)

Fig. 8 (a) Input images (b) their sky regions (white)

$$J_{Non-SKY}(\mathbf{x}) = \frac{1}{t'(\mathbf{x})} \{ (I_c(\mathbf{x}) - I_{SKY}(\mathbf{x})) - A_c \} + A_c \quad (9)$$

Finally, we employ the alpha blending technique as shown in Eq. (10) so as to naturally join the sky and non-sky regions. Through the Gaussian filtering, the sky area and the non-sky area are connected more naturally.

$$J(\mathbf{x}) = I_{MAP}(\mathbf{x}) \cdot J_{SKY}(\mathbf{x}) + (1 - I_{MAP}(\mathbf{x})) \cdot J_{Non-SKY}(\mathbf{x}) \quad (10)$$

where $I_{MAP}(\mathbf{x})$ indicates the sky binary map such as Fig. 8 (b).

4. Experiment and Results

For the following experiments, the test videos consist of 10 sets of fog-free videos and 15 sets of foggy videos, all of which have a 720p@30Hz resolution. Also, all video sets are composed of 1,500 frames each. Fog-free videos were obtained through Youtube, and foggy videos were taken using Apple's iPhone 6 by ourselves. The vanishing point for the ROI setting was set manually for all the video sequences. The proposed fog detection algorithm written in C has a very fast processing speed of 0.07ms per frame on a PC platform having Intel Core i7 CPU and RAM of 32GB. Note that our algorithm operates only on CPU.

First, the proposed fog detection algorithm was compared with the Mao et al.'s method [12]. For performance comparison, we implemented Mao et al.'s method directly using C. Next, in order to examine applicability of the proposed method, the fog removal results using several de-fogging methods were compared in terms of subjective image quality.

4.1 Evaluation of Fog Detection Performance

Detection accuracy of the proposed fog detection algorithm was examined according to W . The results are shown in Table 2. For the fog free images as well as the foggy images, the proposed detection algorithm showed an accuracy of more than 97%.

Next, we compared the proposed method with one of the latest single image-based fog detection methods, Mao et al. [12]. When the parameters given in [12] are used as

Table 2 Accuracy of fog detection

| Test image | Proposed method | | | | Mao' method | |
|----------------|-----------------|--------|--------|---------|-------------------|-----------------|
| | $W=15$ | $W=30$ | $W=60$ | $W=120$ | Default parameter | Tuned parameter |
| Fog-free image | 98.15% | 98.33% | 98.01% | 97.67% | 66.37% | 94.38% |
| Foggy image | 98.74% | 98.82% | 99.06% | 99.37% | 100% | 89.88% |



Fig. 9 Examples of test foggy images. (a) Test image 1 ($R_j = 15.9$) (b) test image 2 ($R_j = 30.3$)

they are, the Mao method shows low detection rate for fog-free images. This is because the Mao et al.'s method defaults to the parameter tuned to the composite images. So we tuned the parameters of the Mao et al.'s method to match the natural foggy images and compared the results. Table 2 shows that the proposed detection algorithm is still better than Mao et al.'s method. Mao et al.'s method has been developed to calculate the fog strength of natural images based on a typical fog model. So, if the sky area occupies a large part of a given image like a road driving image, it is judged that there is a fog even though it is a clear day. On the other hand, since the proposed algorithm estimates the fog strength only for the ROI centered at the vanishing point, it provides relatively more accurate results. In addition, because the proposed algorithm utilizes temporal filtering, it is more robust to outliers.

According to our implementation results, when the input image size is 1280x720, Mao et al.'s method recorded an average operation time per frame of 4.5ms. On the other hand, since the proposed algorithm processes only the ROI region in the center of the input image of the same size, it has an average operation speed of 0.07ms per frame. In other words, the proposed algorithm is about 64 times faster than Mao et al.'s method. Note that the processing times is proportional to the image size.

4.2 Qualitative Evaluation of Defogging with Strength Offset

In this section, when the proposed fog detection algorithm is applied the conventional de-fogging algorithms with the strength offset control, the results are evaluated in terms of subjective image quality. Note that when there is no fog as a result of the fog detection, the de-fogging step is not applied. Also, for foggy images, refer to the fog strength control technique in Sect. 3.2.

In this experiment, the results for two test images with different fog densities of Fig.9 are shown as an example. The α values in Fig.9 were 0.0862 on the left image and 0.0449 on the right image. As de-fogging algorithms, Kim's method, He's method, and Berman's method were considered. First, Fig.10 compares the proposed scheme with Kim's de-fogging method alone. We can observe that the proposed scheme provides a brighter result as shown in Fig. 10 (b) or (d) because of defogging strength.

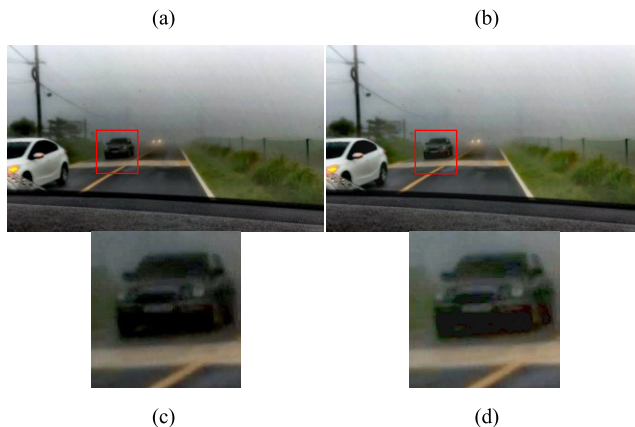
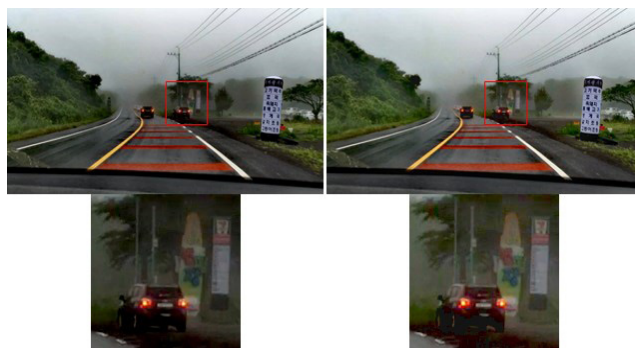


Fig. 10 Results when Kim's method was used. (a) Kim's method alone for test image 1 (b) the proposed scheme for test image 1 (c) Kim's method alone for test image 2 (d) the proposed scheme for test image 2.



Fig. 11 Results when He's method was used. (a) He's algorithm alone for test image 1 (b) the proposed scheme for test image 1 (c) He's algorithm alone for test image 2 (d) the proposed scheme for test image 2.

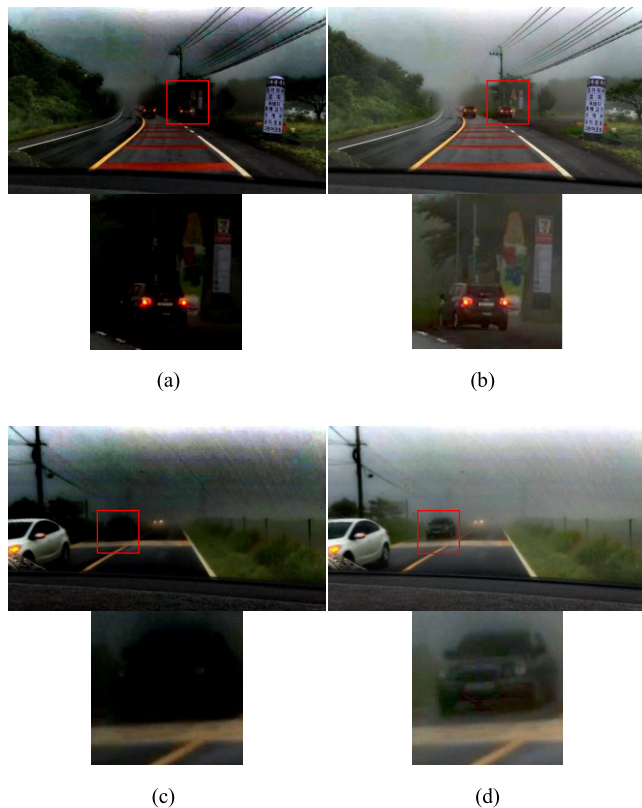


Fig. 12 Results when Berman's method was used. (a) Berman's algorithm alone for test image 1 (b) the proposed scheme for test image 1 (c) Berman's algorithm alone for test image 2 (d) the proposed scheme for test image 2.

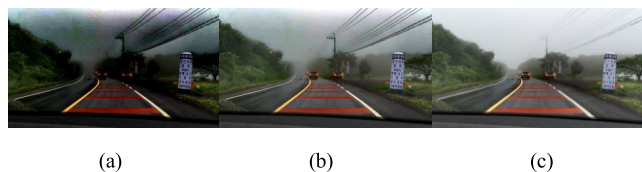


Fig. 13 Results when Berman's method was applied to Fig. 9(a). (a) Berman's algorithm alone for test image 1 (b) the proposed algorithm without sky detection (c) the proposed algorithm with sky detection.

Figure 11 shows the result of applying the proposed scheme to He's algorithm. We can find that the proposed scheme prevents excessive contrast enhancement and improves the image quality by adjusting the brightness. Similarly, Fig. 12 shows a case where the proposed scheme is applied to Berman's de-fogging algorithm. We can observe similar result to Fig. 11.

4.3 Qualitative Evaluation of Defogging with Sky Detection

This subsection evaluates the effect of detection of the sky area and the extra processing on the performance of the proposed algorithm. Here, the Berman's method is again used for fog removal. When de-fogging is performed without sky detection, the sky area is distorted as in Fig. 13 (b). On

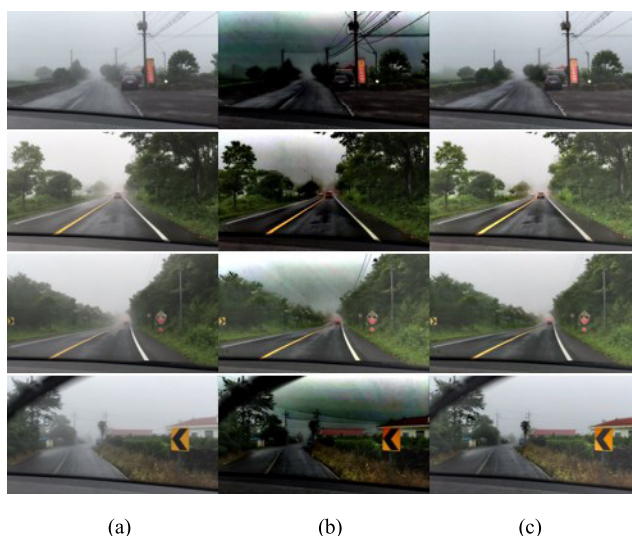


Fig. 14 Effect of sky detection on the overall visual quality. (a) Input images (test images 3-to-6 from the top) (b) the proposed algorithm without sky detection (c) the proposed algorithm with sky detection.

Table 3 Comparison of V/S

| Test image | Fig. 14 (a) | Fig. 14 (c) |
|--------------|-------------|-------------|
| test image 3 | 7.3245 | 3.7719 |
| test image 4 | 3.6251 | 1.7736 |
| test image 5 | 4.9344 | 2.0560 |
| test image 6 | 6.8278 | 2.7123 |

the other hand, when a separate process is performed for the detected sky area, better visual quality is achieved as in Fig. 13 (c). Also, Fig. 14 proves effect of sky detection on the overall visual quality of the proposed algorithm for four different images. In addition, Table 3 shows that $R(f_i)$ dramatically decreases after the proposed fog detection and removal system is applied.

5. Conclusion

In this paper, we propose a novel fog detection algorithm for road driving images. First, a region over a certain distance centered on the vanishing point is set as the ROI. Next, we calculate the average saturation (S) and value (V) ratio in the ROI in the HSV color domain. At this time, temporal filtering is performed on a pre-determined temporal window to minimize the influence of outliers. Finally, fog detection is accomplished by comparing the result with a predetermined threshold. Experimental results of actual photographed images confirmed an accuracy of 97% or more on average. Also, the proposed algorithm shows very fast processing time of about 0.07ms per frame enough to achieve real-time processing, and seldom provides burden to the overall de-fogging system. In addition, we presented a simple method to adjust excessive contrast enhancement during the following de-fogging step, and a region-adaptive de-fogging strategy to avoid too dark output. And, we showed reliable results of the proposed scheme. Thus, the proposed scheme will be a good de-hazing solution of commercial ADAS sys-

tems.

Acknowledgments

This research was supported by National Research Foundation of Korea Grant funded by the Korean Government (2016R1A2B4007353), and was also supported by WCSL (World Class Smart Lab) research grant directed by Inha University.

References

- [1] R.T. Tan, "Visibility in bad weather from a single image," Proc. IEEE Conf. Comput. Vis. Pattern Recog. (CVPR), pp.1–8, June 2008.
- [2] R. Fattal, "Single image dehazing," ACM Trans. Graph., vol.27, no.3, Aug. 2008.
- [3] Q. Zhu, J. Mai, and L. Shao, "A fast single image haze removal algorithm using color attenuation prior," IEEE Trans. Image Process., vol.24, no.11, pp.3522–3533, Nov. 2015.
- [4] K. He, J. Sun, and X. Tang, "Single image haze removal using dark channel prior," IEEE Trans. Pattern Anal. Mach. Intell., vol.33, no.12, pp.2341–2353, Dec. 2011.
- [5] J.-H. Kim, W.-D. Jang, J.-Y. Sim, and C.-S. Kim, "Optimized contrast enhancement for real-time image and video dehazing," J. Vis. Commun. Image Represent., vol.24, no.3, pp.410–425, April 2013.
- [6] D. Berman, T. Treibitz, and S. Avidan, "Non-local image dehazing," Proc. IEEE Conf. Comput. Vis. Pattern Recog. (CVPR), pp.1674–1682, June 2016.
- [7] S.G. Narasimhan and S.K. Nayar, "Vision and the atmosphere," Int'l J. Computer Vision, vol.48, no.3, pp.233–254, 2002.
- [8] M. Pavlic, H. Belzner, G. Rogoll, and S. Ilic, "Image based fog detection in vehicles," IEEE Intelligent Vehicles Symposium, pp.1132–1137, June 2012.
- [9] C. Busch and E. Debes, "Wavelet transform for visibility analysis in fog situations," IEEE Intelligent Systems, vol.13, no.6, pp.66–71, Nov. 1998.
- [10] L. Caraffa and J.P. Tarel, "Daytime fog detection and density estimation with entropy minimization," ISPRS Annals of Photogrammetry, Remote Sensing and Spatial Information Sciences, vol.2, no.3, pp.25–31, Aug. 2014.
- [11] N. Hautière, J.-P. Tarel, H. Halmaoui, R. Brémond, and D. Aubert, "Enhanced fog detection and free space segmentation for car navigation," Machine Vision and Applications, vol.25, no.3, pp.667–679, April 2014.
- [12] J. Mao, U. Phommasak, S. Watanabe, and H. Shioya, "Detecting foggy images and estimating the haze degree factor," Journal of Computer Science & Systems Biology, vol.7, no.6, pp.226–228, 2014.
- [13] C.O. Ancuti, C. Ancuti, C. Hermans, and P. Bekaert, "A fast semi-inverse approach to detect and remove the haze from a single image," Proc. Asian Conf. Comput. Vis. (ACCV), pp.501–514, 2010.
- [14] C. Liu, X. Lu, S. Ji, and W. Geng, "A fog level detection method based on image HSV color histogram," IEEE International Conference on Progress in Informatics and Computing, pp.373–377, May 2014.
- [15] S. Bronte, L.M. Bergasa, and P.F. Alcantarilla, "Fog detection system based on computer vision techniques," Proc. IEEE International Conference on Intelligent Transportation Systems, pp.1–6, Oct. 2009.
- [16] S. Alami, A. Ezzine, and F. Elhassouni, "Local fog detection based on saturation and RGB-correlation," Proc. IEEE International Conference Computer Graphics, Imaging and Visualization, pp.1–5, March 2016.
- [17] H. Kong, J.-Y. Audibert, and J. Ponce, "Vanishing point detection

for road detection," Proc. IEEE Conf. Comput. Vis. Pattern Recog. (CVPR), pp.96–103, June 2009.

- [18] R. Belaroussi and D. Gruyer, "Impact of reduced visibility from fog on traffic sign detection," Proc. IEEE Intelligent Vehicles Symposium, pp.1302–1306, June 2014.
- [19] D. Gruyer, C. Royere, N. du Lac, G. Michel, and J.M. Blosseville, "SiVIC and RTMaps, interconnected platforms for the conception and the evaluation of driving assistance systems," Proc. IEEE Intelligent Transportation Systems World Congress, 5540, Oct. 2006.
- [20] S.S. Agaian, K. Panetta, and A. Grigoryan, "Transform based image enhancement with performance measure," IEEE Trans. Image Processing, vol.10, no.3, pp.367–382, March 2001.
- [21] S.S. Agaian, B. Silver, and K.A. Panetta, "Transform coefficient histogram-based image enhancement algorithms using contrast entropy," IEEE Transactions on Image Processing, vol.16, no.3, pp.741–758, 2007.



Kyeongmin Jeong received his B.S. degree in electronic engineering from Inha University, Incheon, Korea in 2016. Currently, he is pursuing a M.S. degree in electronic engineering from Inha University. His research interests include image processing and computer vision.



Kwangyeon Choi received his B.S. degree and M.S. degree in electronic engineering from Inha University, Incheon, Korea in 2015 and 2017. His research interests include image processing and computer vision.



Donghwan Kim is pursuing a B.S. degree in electronic engineering from Inha University. His research interests include image processing and computer vision.



Byung Cheol Song received the B.S., M.S., and Ph.D. degrees in electrical engineering from the Korea Advanced Institute of Science and Technology (KAIST), Daejeon, Korea, in 1994, 1996, and 2001, respectively. From 2001 to 2008, he was a senior engineer at Digital Media R&D Center, Samsung Electronics Co., Ltd., Suwon, Korea. In March 2008, he joined the Department of Electronic Engineering, Inha University, Incheon, Korea, and currently is a professor. His research interests are in the general areas of image processing and computer vision.